ACS APPLIED MATERIALS & INTERFACES

Research Article

www.acsami.org

Modifications in Morphology Resulting from Nanoimprinting Bulk Heterojunction Blends for Light Trapping Organic Solar Cell Designs

John R. Tumbleston,[†] Abay Gadisa,[‡] Yingchi Liu,[∥] Brian A. Collins,[†,§] Edward T. Samulski,[‡] Rene Lopez,[∥] and Harald Ade*[,†]

[†]Department of Physics, North Carolina State University, Raleigh, North Carolina 27695, United States

[‡]Department of Chemistry and [∥]Department of Physics and Astronomy, University of North Carolina at Chapel Hill, Chapel Hill, North Carolina 27599, United States

Supporting Information

ABSTRACT: Nanoimprinting the photoactive layer of bulk heterojunction (BHJ) organic solar cells is a promising technique for enhancing device performance via improved light absorption. Here, we demonstrate that imprinting poly(3-hexylthiophene) (P3HT) and fullerene BHJ blends leads to adverse morphological changes within the photoactive nanopattern which have been previously overlooked. In particular, nanoimprinting induces a factor of 2 difference in polymer:fullerene composition between the nanopattern posts and interconnecting flash layer that inadvertently moves the composition outside the range for optimal performance. This occurs because of the strong tendency of regioregular P3HT to crystallize since imprinting blends based on amorphous regiorandom P3HT have uniform nanopattern composition. Based on these results, we outline promising design strategies, such as nanoimprinting amorphous polymers, to serve as guidelines for fabricating high-performance nanopatterned BHJ solar cells capable of maximized light absorption.

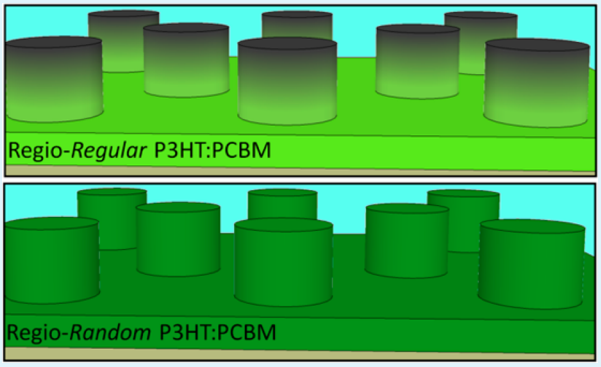

KEYWORDS: *organic solar cells, light trapping, bulk heterojunction morphology, X-ray microscopy, X-ray diffraction, nanoimprinting*

INTRODUCTION

Device performance of polymer:fullerene bulk heterojunction (BHJ) organic solar cells has increased dramatically over the past decade, with power conversion efficiency (PCE) now exceeding 10% for tandem solar cells.[1] Rapid progress has been achieved in part through development of new device designs and architectures. For example, many high-performing devices employ the so-called inverted device design,[2,3] which utilizes more effective electrode interlayers compared to the traditional device configuration. More elaborate architectures have also been developed that employ imprinted or patterned photoactive layers with highly ordered arrays of nonplanar features having periodicities ranging from tens of nanometers to tens of micrometers.[4−6] Motivated by predictions of optical absorption enhancements for feature periodicity on the order of the wavelength of light,[7,8] scalable nanopatterning techniques compatible with roll-to-roll processing have been developed for designs where performance improvements have been noted.[9−12] Nanopatterning has also been used in one of the few BHJ polymer:fullerene solar cells capable of achieving PCE > 8.5%.[13]

In spite of this success, devices incorporating nanopatterns of the most widely used BHJ materials, poly(3-hexylthiophene) (P3HT) and phenyl-C61-butyric acid methyl ester (PCBM),[14−16] do not outperform the best nonpatterned, planar P3HT:PCBM devices.[17,18] While nonuniformities in the built-in electric field of nanoimprinted devices have been investigated,[19,20] the morphological effects of directly imprinting soft, organic materials have been generally overlooked to explain this lack of champion performance. Because nanopattern quality is typically evaluated solely on the basis of feature uniformity using surface-sensitive probes such as scanning electron microscopy (SEM), the characterization of critical imprint-induced morphological properties relevant to performance is often ignored. This includes the polymer:fullerene composition and material crystallinity, both of which could be modified during the imprinting process. It is therefore essential to assess the morphological consequences of nanoimprinting to establish design rules for future devices, and ultimately, to take full advantage of the proven enhancements in light absorption.

Herein, we demonstrate that nanoimprint lithography induces compositional variations in photoactive submicrometer patterns comprised of regioregular (RReg) P3HT as electron

Received: June 18, 2013
Accepted: August 2, 2013
Published: August 2, 2013

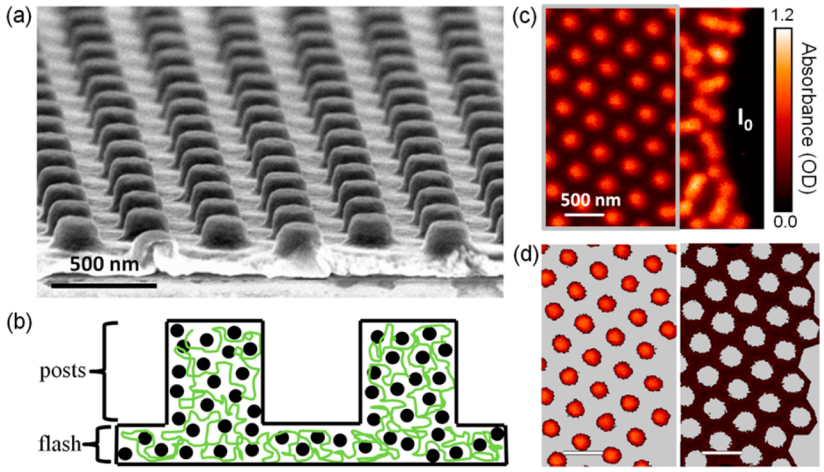

Figure 1. (a) SEM image of nanoimprinted RReg P3HT:PCBM photoactive layer. The nanopatterns comprise posts spaced by 400 nm in a hexagonal array with 200 nm diameters. (b) Adjacent posts are connected by a flash layer, where P3HT polymer chains are green and PCBM molecules are black spheres (not to scale). (c) Optical absorbance of photoactive nanopattern for 284.4 eV incident photon energy acquired with STXM. Within the image, a sample-free area is used to simultaneously measure the incident photon flux, I_0. (d) Masks that isolate posts (left) and the exposed flash (right) are used to determine the average absorbance in the posts and flash layer, respectively.

donor and PCBM as electron acceptor. Using scanning transmission X-ray microscopy (STXM), we show that 200 nm diameter nanopatterned posts have a higher concentration of PCBM than the underlying "flash" layer that connects adjacent posts (see Figure 1) leaving the flash layer below the optimum composition for high performance.[21,22] This occurs at the standard temperatures used for nanoimprinting but is less severe when the fabrication temperature is reduced. No compositional differences are found in nanoimprinted blends comprised of amorphous regiorandom (RRan) P3HT and PCBM supporting the conclusion that the composition variations in RReg P3HT nanopatterns are likely related to the strong tendency for RReg P3HT to crystallize. Along with composition, the relative orientation of RReg P3HT polymer crystallites with respect to the substrate is also modified, exhibiting greater face-on orientation with nanoimprinting. Overall, crystallinity is an important material property to consider when evaluating the potential for a nanopatterned BHJ system to be successful. Our findings suggest that photovoltaic devices produced from low crystallinity polymers are more likely to benefit from nanoimprinting.

EXPERIMENTAL SECTION

Sample Preparation: P3HT was purchased from Rieke Metals (regioregular, $M_w \approx$ 41K; PDI, 2.0; regioregularity, 93%; and regiorandom, $M_w \approx$ 80K). PCBM was purchased from Nano-C (99.5% purity). All materials were used as received. P3HT:PCBM films were spuncast from a dichlorobenzene solution using a 1:0.8 w/w ratio solution for RReg P3HT and 1:1 ratio for RRan P3HT. Films were cast on PSS-coated glass substrates for STXM measurement and PSS-coated Si substrates for GIWAXS measurement. Nanopatterns were fabricated using Pattern Replication in Nonwetting Templates (PRINT) with an elastomeric molding material based on perfluoropolyether (PFPE) in a nitrogen-filled glovebox. Films were also nanoimprinted at room temperature outside the glovebox in a closed container into which nitrogen was used as a carrier for solvent vapor.

X-ray Characterization and Analysis: STXM was conducted at Beamline 5.3.2.2 of the Advanced Light Source (ALS). Nanopatterns prepared on PSS-coated glass substrates were floated onto TEM grids. During measurement, the chamber was filled with 1/3 ATM He. GIWAXS was carried out at Beamline 7.3.3 of the ALS using a Dectris Pilatus 1 M photon counting detector. Samples were measured at an incident angle of 0.15°, above the critical angle so the X-ray beam penetrated to the substrate. The photon energy used for GIWAXS was 10 keV. Air scatter, which contributes a background signal, was reduced using helium gas. An assumed density of 1.2 g/cm^3 was used to calculate the thickness maps from STXM imaging (Figure 3) for both RRan P3HT:PCBM and RReg P3HT:PCBM.

RESULTS AND DISCUSSION

Nanopatterns of RReg P3HT:PCBM blends were fabricated using pattern replication in nonwetting templates (PRINT).[23] Submicrometer post arrays of P3HT:PCBM have been previously fabricated using this technique,[15] and absorption enhancements have been demonstrated in agreement with predictions from optical models.[8,24] Imprinting P3HT:PCBM with other low surface energy materials, such as polydimethylsiloxane (PDMS), has also been reported.[14,16] Figure 1a shows PRINT nanopatterns of P3HT:PCBM imaged using SEM. A hexagonal lattice of posts is formed with a nearest neighbor center-to-center distance of 400 nm and post diameter of 200 nm. Connecting each of the posts is a flash layer as labeled in Figure 1b. During the nanoimprinting process, the PFPE mold is pressed into a previously spuncast P3HT:PCBM film under elevated temperature or in the presence of a saturated solvent atmosphere (discussed below).

Although excellent nanopattern uniformity is obtained, SEM and other scanning probe techniques such as atomic force microscopy are not sensitive to potential compositional variations across the nanoimprinted material (posts versus flash layer). Even though the surface energy of the PFPE stamp is very low, there could still be unintentional preferential migration of one component since the tangled P3HT polymers are less mobile than PCBM small molecules. To address this possibility, composition is measured using scanning transmission X-ray microscopy (STXM), which utilizes the near edge X-ray absorption fine structure (NEXAFS) spectra of P3HT and PCBM that have unique spectral features near the carbon 1s absorption edge. STXM was conducted at Beamline 5.3.2.2 of the Advanced Light Source[25] (see the Supporting Information for measurement details). This technique has been previously used to measure absolute composition of PCBM in P3HT films[26,27] and the composition of other BHJ blends.[28−30]

Moreover, STXM can resolve features below 50 nm. The combination of high resolution and material sensitivity makes this spectromicroscopy tool an excellent technique to assess compositional differences in nanoimprinted photoactive layers with submicrometer sized features.

Figure 1c shows optical absorbance of a nanopatterned sample for 284.4 eV incident photon energy. The black area on the right side of the image is an area with no sample, so the incident photon flux (I_0) can be simultaneously measured to obtain the optical absorbance. Individual posts are clearly resolved with the same feature size and spacing as observed in the SEM image (Figure 1a). Differences in optical absorbance are a combination of two effects dictated by the Beer−Lambert law. First, thickness differences between the posts and the flash layer will change the absorbance and second, compositional variations will also lead to absorbance differences depending on the photon energy. The average absorbance is determined separately for posts and regions of the flash layer that are post-free using masks based on histograms of detector counts (Figure 1d). It should be noted that the STXM measurement is done in transmission, so any vertical composition variations will be averaged.

Because a single energy is not enough to distinguish between thickness and compositional differences, ∼40 images with different photon energies were acquired to produce average absorbance spectra that represent the post areas and flash layer, respectively. These spectra are shown in Figure 2 for three different nanoimprinting temperatures. Also shown in Figure 2b are the measured pure material NEXAFS reference spectra of P3HT and PCBM, which reveal the unique spectral fingerprints of each material. Near the absorption edge, the spectra are very different, while well above the edge (e.g., 320 eV), the intrinsic absorption of P3HT and PCBM is similar. Differences in the measured post and flash spectra for each imprinting temperature are noted especially near the PCBM absorption peak (∼284 eV) where the absorbance is greater for the posts than for the flash layers in all samples. Using the pure material spectra, the absorbance data are fit using an overall scaling factor to account for thickness variations along with a weighted linear combination of the reference spectra following previous methods.[31] Fits are achieved that capture the essential features of the data. As a check, measurement of a nonpatterned, planar P3HT:PCBM film resulted in a PCBM weight percentage of 42.4%, which is close to the nominal 44.4% expected from the 1:0.8 wt. ratio solution used (see the Supporting Information, Figure S1). It should also be noted that the P3HT pure material reference spectrum used in the fits was acquired from a spuncast film pressed with a featureless (i.e., flat) PFPE mold and is different than a spectrum from a standard spuncast only film (see the Supporting Information, Figure S2). Using either spectrum does not significantly alter the fitted values, but a better fit is achieved using the spectrum corresponding to the pressed P3HT. Finally, an anisotropy factor that accounts for polymer orientational differences is also used in the fit, following previous protocols for fitting P3HT:PCBM composition.[27]

The fits in Figure 2 reveal that the content of PCBM in the posts is twice the amount by weight than in the flash layer for the nanopattern produced under standard processing conditions at 140 °C. Furthermore, given the nominal value of PCBM of 44% based on the solution weight ratio, it is apparent that some PCBM is removed during the nanoimprinting process. This leaves the composition in the flash layer much

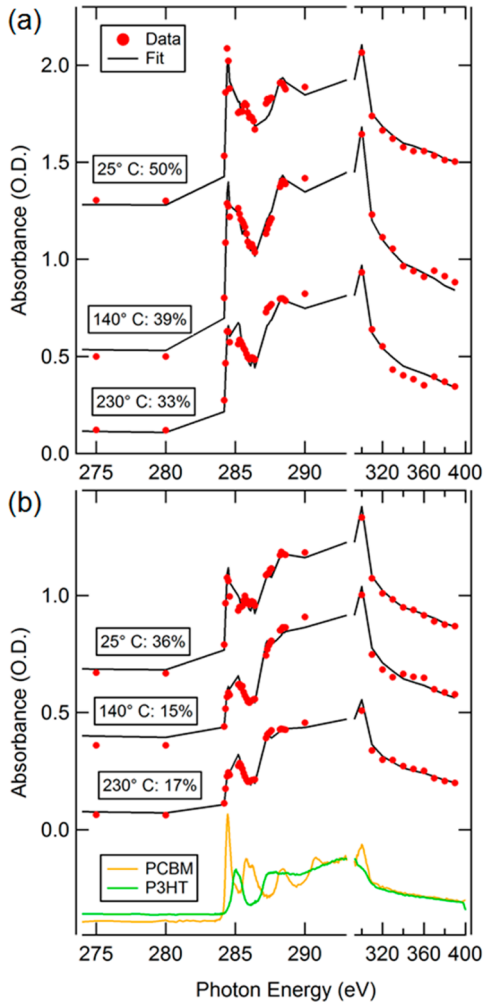

Figure 2. Measured absorbance and composition fits for (a) post areas and (b) exposed flash layer for nanopatterns imprinted at different temperatures. Absorbance for each energy corresponds to a separate image using the masking technique described in Figure 1. For all temperatures, there is higher PCBM percentage by weight in the posts than in the flash layer as labeled. This leads to flash layer composition that is below the optimum for high performance. The spectra for 140° and 25 °C are vertically offset for clarity. Pure material NEXAFS reference spectra for P3HT and PCBM with unique spectral fingerprints are also shown in b.

lower than the optimum range for high performance between 40 and 50% PCBM.[21,22] The amount of loss decreases with decreasing temperature and is the least for samples imprinted at room temperature using a saturated solvent atmosphere. We hypothesize that the PCBM is transferred to the mold, which is a function of temperature. Interestingly, there are still compositional differences between the posts and flash layer even when imprinting without elevated temperature. However, the composition remains nearly inside the range of optimum composition for high performance and should not be detrimental.

These results are unexpected and reveal that the composition can differ substantially across nanopatterned photoactive layers. Along with the nanoimprinting temperature, the extent of compositional heterogeneity is potentially related to the material properties of the chosen polymer and fullerene. To test the influence of polymer crystallinity in particular, nanopatterns were fabricated using a BHJ film of highly

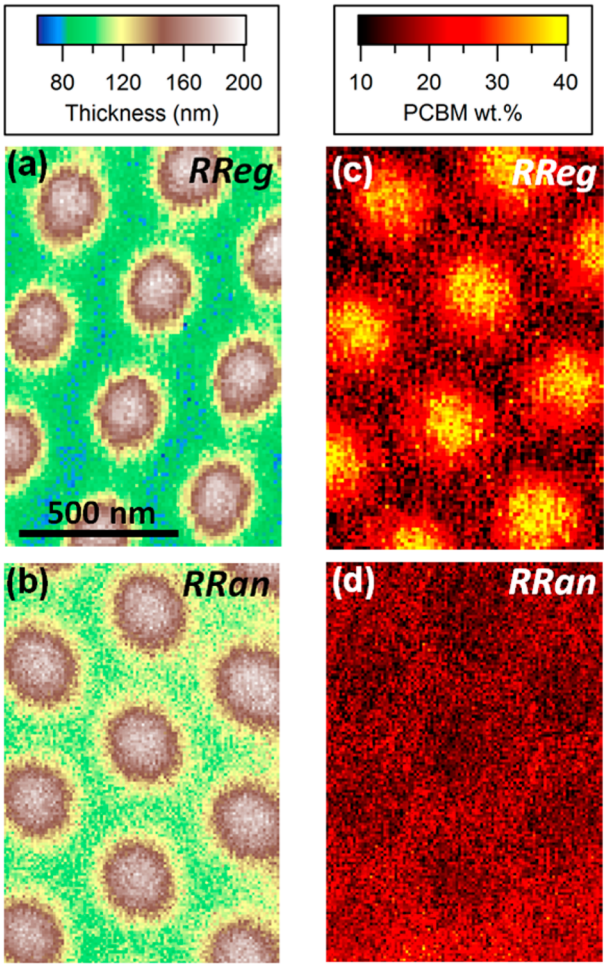

Figure 3. (a, b) Thickness and (c, d) composition maps derived from STXM measurements of nanopatterns comprised of PCBM and (a, c) RReg P3HT and (b, d) RRan P3HT. Both nanopatterns are fabricated at 140 °C. The composition differences between the posts and the flash layer are minimal in the nanopattern made with amorphous RRan P3HT compared to the nanopattern made with semicrystalline RReg P3HT.

amorphous RRan P3HT with PCBM at 140 °C. Thickness and composition maps are displayed in Figure 3 comparing nanopatterns made with RRan P3HT to those made with RReg P3HT. The maps are calculated using two STXM images with different energy (284.4 and 320 eV in this case) following previous methodology.[30] The thickness maps reveal similar feature height, size, and spacing for both RReg and RRan P3HT:PCBM nanopatterns (Figure 3a, b), supporting the effectiveness of the PRINT technique regardless of material choice. However, in terms of composition, the RReg P3HT:PCBM pattern (Figure 3c) exhibits differences between the posts and flash layer, in agreement with the fits in Figure 2. On the other hand, the composition map for the RRan P3HT:PCBM nanopattern (Figure 3d) shows minimal composition differences between the posts and flash layer. While there is still some PCBM mass loss during nanoimprinting, there is not a drastic compositional difference between the posts and flash layer like for the RReg P3HT:PCBM nanopattern. This was also the case when imprinting at other temperatures with RRan P3HT (data not shown here). These results indicate that RRan P3HT is not as susceptible to composition variations during the nanoimprinting process.

The primary difference between RReg P3HT and RRan P3HT is their tendency, or lack thereof, to crystallize. RRan P3HT is highly amorphous, while RReg P3HT readily crystallizes. The differences in crystallinity were assessed with grazing incidence wide-angle X-ray scattering (GIWAXS) conducted at Beamline 7.3.3 of the Advanced Light Source.[32] Figure 4 shows an absence of P3HT crystal peaks for the RRan P3HT:PCBM nanopattern as expected, while the RReg P3HT:PCBM nanopattern exhibits P3HT crystallite reflections in both the lamellar (h00) and $\pi-\pi$ stacking (0k0) directions (Figure 4). RReg P3HT is a highly semicrystalline material for

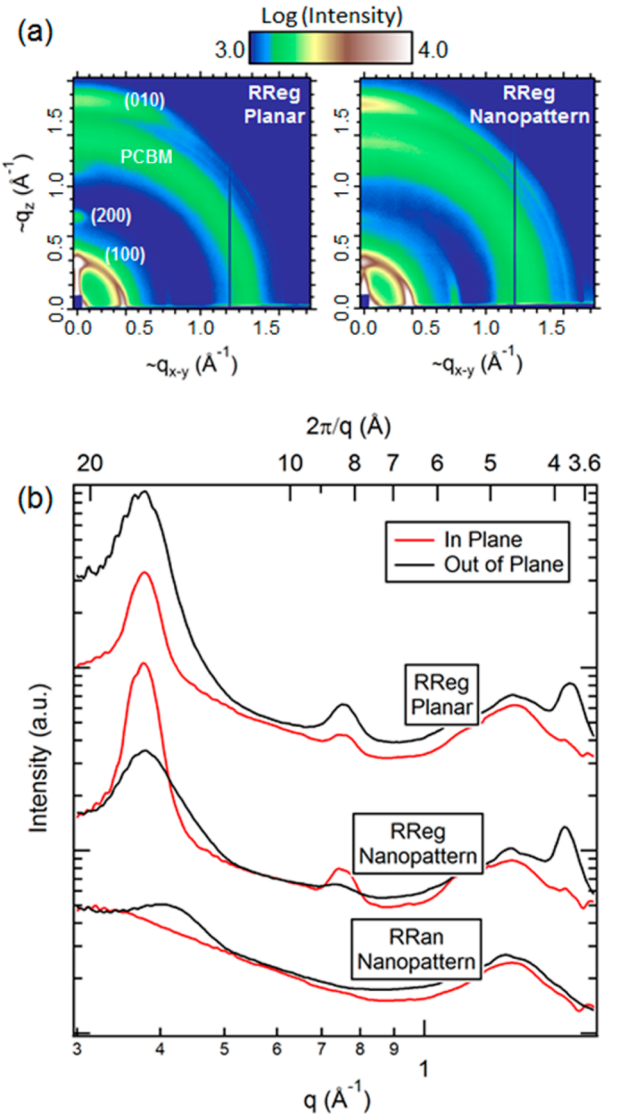

Figure 4. (a, b) GIWAXS scattering data for (left) nonpatterned, planar RReg P3HT:PCBM and (right) RReg P3HT:PCBM nanopatterned samples, with the important peaks labeled. (b) In sample plane and out-of-plane sector averages reveal that nanoimprinting causes P3HT crystals to become more face-on with respect to the substrate compared to the nonpatterned planar film. Sector averages are also shown for the RRan P3HT:PCBM nanopatterned sample that lacks crystal reflections. It should be noted that (a) are not corrected for the missing wedge in the out-of-plane direction, making the axes approximate.

dx.doi.org/10.1021/am402363r | ACS Appl. Mater. Interfaces 2013, 5, 8225−8230

which the crystallization dynamics play an important role in influencing the morphological development of BHJ blends.[33,34] The crystallization of P3HT also plays an important role in the compositional measurements shown in Figures 2 and 3. We rationalize the observations as follows. The crystallization of RReg P3HT makes this material very immobile compared to dispersed PCBM molecules that can move freely, especially at elevated temperature.[35] The RReg P3HT crystals thus form a rigid matrix during the nanoimprinting process where the crystallites are unable to fill the mold voids effectively, leaving them open to excess PCBM infiltration.

Also noted from Figure 4 are differences in the diffraction between a nonpatterned, planar RReg P3HT:PCBM thin film and a nanopatterned one. The planar film has more intense lamellar reflections in the out of sample plane direction ($\sim q_z$) compared to in plane ($\sim q_{x\text{-}y}$) as expected.[34] On the other hand, the nanopatterned sample has higher intensity lamellar reflections in the in plane compared to the out of plane direction (see the Supporting Information, Figure S3, for multipeak fits). This indicates a reorientation of P3HT crystallites to be comparatively more face-on with respect to the substrate with nanoimprinting. In other words, a higher proportion of polymer crystallites are oriented with side chains parallel to the substrate for the patterned sample compared to the nonpatterned control. The fraction of P3HT near the mold interface in the posts likely increases the face-on signal. Reorientation of P3HT crystallites in nanopatterns based solely on RReg P3HT has been recently reviewed,[6] where an enhancement in face-on population as observed here was previously shown in nanogratings of P3HT.[36] A higher population of face-on crystallites with out of plane $\pi-\pi$ stacking could improve vertical charge transport[37] for nanoimprinted blends, but this benefit would compete against the negative impact of the compositional heterogeneities discussed above.

The compositional variations described above induced by the strong propensity of RReg P3HT to crystallize help explain the inability of nanopatterned RReg P3HT:PCBM devices to outperform the best nonpatterned P3HT:PCBM devices in literature. This prompts us to suggest three design rules that can be followed to fabricate devices with nanopatterned photoactive layers capable of converting enhanced light absorption to enhanced photocurrent: (1) Nanoimprint amorphous materials. It is encouraging that the highest performing BHJ polymer to date, PTB7,[2] is highly amorphous[30] and has been recently used in initial work to fabricate photoactive nanopatterns.[38] (2) Nanoimprint other sublayers of the solar cell and then use standard casting of the photoactive layer. This has been successfully demonstrated for RReg P3HT:PCBM with PCE > 4.0%[20] along with other BHJ blends.[11] (3) Nanoimprint the photoactive layer at low temperature, potentially with the aid of a solvent-saturated atmosphere. Along with its likely amorphous structure based on a similar polymer,[39] the previously mentioned nanopatterned device with PCE > 8.5% was imprinted at room temperature. Quenching from a melt at high temperature should also mitigate compositional variations when using semicrystalline materials. Furthermore, limiting the number of tie chains between crystallites by controlling the polymer molecular weight may also make semicrystalline polymers easier to deform plastically.[40]

CONCLUSIONS

In summary, nanoimprinting submicrometer features in highly crystalline materials, such as RReg P3HT:PCBM, results in compositional heterogeneity which, in turn, has negative consequences for solar cell efficiency. The compositional differences between the posts and flash layer can be mitigated by using a highly amorphous polymer, such as PTB7. On the other hand, if a highly crystalline polymer is used, like RReg P3HT, then nanoimprinting should be conducted at room temperature. If the induced compositional variations are within the range corresponding to high performance, then there is the potential added benefit of higher mobility in the direction of charge transport due to a greater population of polymer crystals taking a face-on orientation with respect to the substrate. Overall, these results suggest fabrication strategies for maximizing light absorption and efficiency in high-performance organic solar cells with nanopatterned photoactive layers.

ASSOCIATED CONTENT

Supporting Information

Sample preparation details, measurement procedures, P3HT reference spectra comparison, and GIWAXS multipeak fits. This material is available free of charge via the Internet at http://pubs.acs.org/.

AUTHOR INFORMATION

Corresponding Author

*E-mail: harald_ade@ncsu.edu.

Present Address

[§]Material Science and Engineering Division, National Institute of Standards and Technology, Gaithersburg, Maryland 20899, United States

Notes

The authors declare no competing financial interest.

ACKNOWLEDGMENTS

J.R.T., B.A.C., and H.A. were supported by DOE, OS, BES, MSE (DE-FG02-98ER45737). Data were acquired at beamlines 5.3.2.2 and 7.3.3 of the ALS, which is supported by DOE (DE-AC02-05CH1123). Work by A.G., Y.L., E.T.S., and R.L. was supported by NSF (Solar:DMR-0934433). Thanks are given to David Kilcoyne at beamline 5.3.2.2 and Alexander Hexemer, Eric Schaible, and Steven Alvarez at beamline 7.3.3 for assistance with data acquisition.

REFERENCES

(1) You, J.; Dou, L.; Yoshimura, K.; Kato, T.; Ohya, K.; Moriarty, T.; Emery, K.; Chen, C.-C.; Gao, J.; Li, G.; Yang, Y. *Nat. Commun.* **2013**, *4*, 1446.

(2) He, Z.; Zhong, C.; Su, S.; Xu, M.; Wu, H.; Cao, Y. *Nat. Photon.* **2012**, *6*, 591−595.

(3) Small, C. E.; Chen, S.; Subbiah, J.; Amb, C. M.; Tsang, S.-W.; Lai, T.-H.; Reynolds, J. R.; So, F. *Nat. Photon.* **2012**, *6*, 115−120.

(4) Ko, D. H.; Tumbleston, J. R.; Gadisa, A.; Aryal, M.; Liu, Y. C.; Lopez, R.; Samulski, E. T. *J. Mater. Chem.* **2011**, *21*, 16293−16303.

(5) Escoubas, L.; Simon, J.-J.; Torchio, P.; Duché, D.; Vedraine, S.; Vervisch, W.; Le Rouzo, J.; Flory, F.; Rivière, G.; Yeabiyo, G.; Derbal, H. *Appl. Opt.* **2011**, *50*, C329−C339.

(6) Yang, Y.; Mielczarek, K.; Aryal, M.; Zakhidov, A.; Hu, W. *ACS Nano* **2012**, *6*, 2877−2892.

(7) Duche, D.; Escoubas, L.; Simon, J.-J.; Torchio, P.; Vervisch, W.; Flory, F. *Appl. Phys. Lett.* **2008**, *92*, 193310.

(8) Tumbleston, J. R.; Ko, D. H.; Samulski, E. T.; Lopez, R. *Appl. Phys. Lett.* **2009**, *94*, 043305.
(9) Ko, D. H.; Tumbleston, J. R.; Zhang, L.; Williams, S.; DeSimone, J. M.; Lopez, R.; Samulski, E. T. *Nano Lett.* **2009**, *9*, 2742−2746.
(10) Nalwa, K. S.; Park, J.-M.; Ho, K.-M.; Chaudhary, S. *Adv. Mater.* **2010**, *23*, 112−116.
(11) Wang, D. H.; Seifter, J.; Park, J. H.; Choi, D.-G.; Heeger, A. J. *Adv. Energy Mater.* **2012**, *2*, 1319−1322.
(12) Li, K.; Zhen, H.; Huang, Z.; Li, G.; Liu, X. *ACS Appl. Mater. Interfaces* **2012**, *4*, 4393−4397.
(13) Li, X.; Choy, W. C. H.; Huo, L.; Xie, F.; Sha, W. E. I.; Ding, B.; Guo, X.; Li, Y.; Hou, J.; You, J.; Yang, Y. *Adv. Mater.* **2012**, *24*, 3046−3052.
(14) Na, S.-I.; Kim, S.-S.; Jo, J.; Oh, S.-H.; Kim, J.; Kim, D.-Y. *Adv. Funct. Mater.* **2008**, *18*, 3956−3963.
(15) Ko, D.-H.; Tumbleston, J. R.; Schenck, W.; Lopez, R.; Samulski, E. T. *J. Phys. Chem. C* **2011**, *115*, 4247−4254.
(16) Li, X. H.; Sha, W. E. I.; Choy, W. C. H.; Fung, D. D. S.; Xie, F. X. *J. Phys. Chem. C* **2012**, *116*, 7200−7206.
(17) Li, G.; Shrotriya, V.; Huang, J. S.; Yao, Y.; Moriarty, T.; Emery, K.; Yang, Y. *Nat. Mater.* **2005**, *4*, 864−868.
(18) Dang, M. T.; Hirsch, L.; Wantz, G. *Adv. Mater.* **2011**, *23*, 3597−3602.
(19) Vervisch, W.; Riviere, G.; Vedraine, S.; Biondo, S.; Torchio, P.; Duche, D.; Simon, J.-J.; Escoubas, L. *J. Appl. Phys.* **2012**, *111*, 094506.
(20) Liu, Y.; Kirsch, C.; Gadisa, A.; Aryal, M.; Mitran, S.; Samulski, E. T.; Lopez, R. *J. Phys. D: Appl. Phys.* **2013**, *46*, 024008.
(21) Müller, C.; Ferenczi, T. A. M.; Campoy-Quiles, M.; Frost, J. M.; Bradley, D. D. C.; Smith, P.; Stingelin-Stutzmann, N.; Nelson, J. *Adv. Mater.* **2008**, *20*, 3510−3515.
(22) Moule, A. J.; Bonekamp, J. B.; Meerholz, K. *J. Appl. Phys.* **2006**, *100*, 094503.
(23) Rolland, J. P.; Maynor, B. W.; Euliss, L. E.; Exner, A. E.; Denison, G. M.; DeSimone, J. M. *J. Am. Chem. Soc.* **2005**, *127*, 10096−10100.
(24) Tumbleston, J. R.; Ko, D. H.; Samulski, E. T.; Lopez, R. *Opt. Express* **2009**, *17*, 7670−7681.
(25) Kilcoyne, A. L. D.; Tyliszczak, T.; Steele, W. F.; Fakra, S.; Hitchcock, P.; Franck, K.; Anderson, E.; Harteneck, B.; Rightor, E. G.; Mitchell, G. E.; Hitchcock, A. P.; Yang, L.; Warwick, T.; Ade, H. *J. Synchrotron. Radiat.* **2003**, *10*, 125−136.
(26) Watts, B.; Belcher, W. J.; Thomsen, L.; Ade, H.; Dastoor, P. C. *Macromolecules* **2009**, *42*, 8392−8397.
(27) Collins, B. A.; Gann, E.; Guignard, L.; He, X.; McNeill, C. R.; Ade, H. *J. Phys. Chem. Lett.* **2010**, *1*, 3160−3166.
(28) McNeill, C. R.; Watts, B.; Thomsen, L.; Belcher, W. J.; Kilcoyne, A. L. D.; Greenham, N. C.; Dastoor, P. C. *Small* **2006**, *2*, 1432−1435.
(29) McNeill, C. R.; Watts, B.; Thomsen, L.; Belcher, W. J.; Greenham, N. C.; Dastoor, P. C. *Nano Lett.* **2006**, *6*, 1202−1206.
(30) Collins, B. A.; Li, Z.; Tumbleston, J. R.; Gann, E.; McNeill, C. R.; Ade, H. *Adv. Energy Mater.* **2013**, *3*, 65−74.
(31) Collins, B. A.; Ade, H. *J. Electron Spectrosc. .* **2012**, *185*, 119−128.
(32) Hexemer, A.; Bras, W.; Glossinger, J.; Schaible, E.; Gann, E.; Kirian, R.; MacDowell, A.; Church, M.; Rude, B.; Padmore, H. *J. Phys. Conf. Ser.* **2010**, *247*, 012007.
(33) Chen, D.; Liu, F.; Wang, C.; Nakahara, A.; Russell, T. P. *Nano Lett.* **2011**, *11*, 2071−2078.
(34) Collins, B. A.; Tumbleston, J. R.; Ade, H. *J. Phys. Chem. Lett.* **2011**, *2*, 3135−3145.
(35) Treat, N. D.; Brady, M. A.; Smith, G.; Toney, M. F.; Kramer, E. J.; Hawker, C. J.; Chabinyc, M. L. *Adv. Energy Mater.* **2011**, *1*, 82−89.
(36) Hlaing, H.; Lu, X.; Hofmann, T.; Yager, K. G.; Black, C. T.; Ocko, B. M. *ACS Nano* **2011**, *5*, 7532−7538.
(37) Sirringhaus, H.; Brown, P. J.; Friend, R. H.; Nielsen, M. M.; Bechgaard, K.; Langeveld-Voss, B. M. W.; Spiering, A. J. H.; Janssen, R. A. J.; Meijer, E. W.; Herwig, P.; De Leeuw, D. M. *Nature* **1999**, *401*, 685−688.
(38) You, J.; Li, X.; Xie, F.-X.; Sha, W. E. I.; Kwong, J. H. W.; Li, G.; Choy, W. C. H.; Yang, Y. *Adv. Energy Mater.* **2012**, *2*, 1203−1207.
(39) Huang, Y.; Guo, X.; Liu, F.; Huo, L.; Chen, Y.; Russell, T. P.; Han, C. C.; Li, Y.; Hou, J. *Adv. Mater.* **2012**, *24*, 3383−3389.
(40) Ro, H. W.; Akgun, B.; O'Connor, B. T.; Hammond, M.; Kline, R. J.; Snyder, C. R.; Satija, S. K.; Ayzner, A. L.; Toney, M. F.; Soles, C. L.; DeLongchamp, D. M. *Macromolecules* **2012**, *45*, 6587−6599.